Experimental Measurements of Overload and Underloads on Fatigue Crack Growth Using Digital Image Correlation

Paul A. Lara, Hugh A. Bruck, and Felix J. Fillafer

Abstract Aluminum materials are utilized across many industries, spanning from the cycling, automotive, aerospace, and the marine industry. In the latter, marine grade aluminum materials are utilized to construct the hull, appendages, and/or specific components. In particular, 5xxx series aluminum materials are relied on by the marine industry for these purposes, where their material properties are advantageous to reducing the overall weight of naval platforms and reducing their operational cost. During its lifetime, a marine vessel will experience a multitude of variable amplitude loading conditions, with occasional overloads and underloads depending on the sea environment encountered. In some cases, these overloads/underloads result affect the catastrophic failure of the structure and associated design lifetime due to changes in the crack growth rate in 5xxx aluminum materials. Existing models, like the Wheeler, Willemborg, and variations of these, have been utilized to predict the crack growth behavior with varying degrees of success. In this study, we created experimental matrices to explore the effects of overload/underload combinations on fatigue crack growth in 5xxx aluminum. Both visual inspection of crack tip location and Digital Image Correlation (DIC) characterization of the crack tip deformation fields were used to characterize the crack growth in center crack tension (CCT) panel specimens. DIC also enabled additional analysis of strain fields to elucidate on the conditions responsible for the change in the crack growth behavior. Future phases of this work will utilize this data to develop new models for fatigue crack growth.

Keywords Aluminum crack growth · Digital Image Correlation · Center crack tension · Overload · Underload · Plastic zone

Introduction

Embedded high frequency signal effects derived from wave impacts on ships can affect failure mechanisms on the structures and have an adverse impact on the fatigue life of the vessel. While operating in a sea environment, ship structures can be subject to many operational loads (wind, pressure, temperature, etc.), one of which is the structural effects derived from the surrounding sea environment. Typically, the wave environment applies an ordinary wave component which drives the primary bending stress of the vessel, along with a more stochastically driven element that manifest itself as wave impacts. This dynamic wave impacts results in a high frequency vibratory response signals load applied to ship structures. The vibratory nature of these high frequency responses makes the design of structures increasingly complex in nature due to their uncertainty, designers and naval design rule societies have relied on methods such as safety factors and/or margins of safety to account for its effects. A typical wave impact on a Naval Structure imparts a time dependent pulse load that exhibits a higher frequency logarithmic decaying sinusoidal response when measured via experimental means and captured utilizing data acquisition systems. The figure below displays one of these signals, where the measured signal can be decomposed into its different components by applying filtering techniques.

P. A. Lara (✉)
Carderock Division, Naval Surface Warfare Center, West Bethesda, MD, USA
e-mail: paul.lara@navy.mil

H. A. Bruck
Mechanical Engineering Department, University of Maryland, College Park, MD, USA

F. J. Fillafer
Mannheim University of Applied Science, Mannheim, Germany

M. Silberstein et al. (eds.), *Challenges in Mechanics of Time Dependent Materials, Fracture, Fatigue, Failure and Damage Evolution, Volume 2*, Conference Proceedings of the Society for Experimental Mechanics Series, https://doi.org/10.1007/978-3-030-29986-6_5

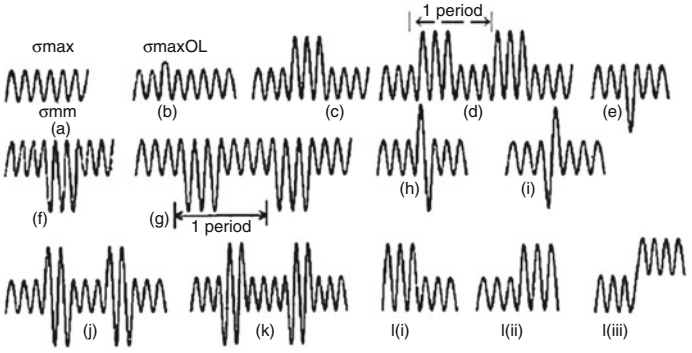

(a) CAL;typical VAL sequences; (b) single Ol; (c) block of OL; (d) period blocks of OL; (e) single UL; (f) block of UL; (g) period blocks of UL; (h) single OL-UL; (i) single UL-OL; (j) periodic OL-UL blocks; (k) periodic UL-OL blocks; and (l) two-level block loading -l(i) high-low; (ii) low-high; and l(iii) both maximum and minimum load

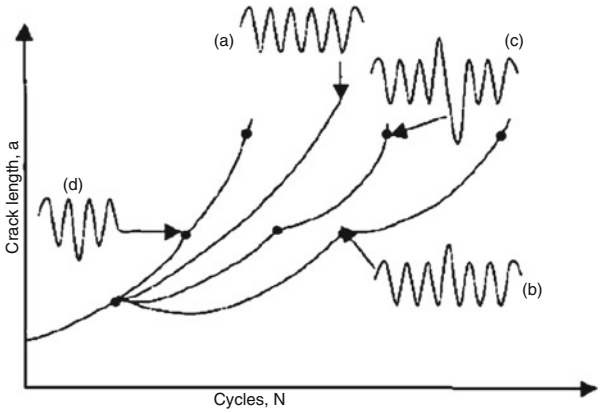

Figure 3 Transient effects on crack growth produced by (a) CAL; (b) single overload; (c) tensile-compressive overload sequence; and (d) single underload

Fig. 1 Load Sequencing [2]

Under the current practices, the peaks of these responses are utilized to compare to the quasi-static design stresses, as well as evaluate the fatigue life of the structures either under constant or variable amplitude experimentation. Figure 1 above displays this kind of behavior, where underloads and underloads affect the crack growth rate behavior of material under a simplified signal approach [1].

But there are additional higher frequency characteristics to these high frequency signals are not currently taken into consideration. Existing academic research has been centered on capturing a simplified sinusoidal response associated with this slamming event and embedded high frequency response, but has not addressed logarithmic decay, signal frequency, or frequency of occurrence. Work by Sumi et al. has centered on more complex signals, where bounding functions where used to predict crack growth behavior [2], and the results show an influence of crack length predictions based on utilizing these bounding functions.

All these factors have associated uncertainty and cause impact on fatigue life and failure mechanisms exhibited by ship structures, work by researchers such as Fricke et al. has shown damage variation as related to amplitude of high frequency signals [3]. The work presented is a multiphase task that looks to gather fundamental understanding of the effects of this high frequency loading on Aluminum 5xxx material, accounting for some of the signal's characteristics, and through an experimental evaluation assess its impact on the local failure mechanism and life cycle models. The foundational findings of this research, can then be used in future investigative efforts to develop analytical models addressing heat affected zones, provide underpinnings for high fidelity numerical modelling, eventually providing broader toolsets to designers that can be used to reduce the dependency on safety factors and introduce more rigorous failure mechanism design criterion. The presented work has the following two basic research objectives: develop and execute an experimental evaluation matrix to investigate a bound set of effects of embedded high frequency signals on fatigue crack growth and associated initiation of failure, and develop failure models that incorporate uncertainty in signal parameters variation and their associated influence on material failure. The first is presented as part of this work, and the latter to be presented as part of future efforts.

Experiment Design

This work builds and complements on existing work developed by Hart and Bruck [4] where the investigators looked at failure of aluminum 5052-H32 and the applications of composite patches to aluminum and the effects of crack growth. Whereas their work centered on the utilization of a composite laminate to mitigate crack growth on ultimate failure, this work looks at the effects of crack growth based on loading condition. Figure 2 below displays the aluminum material properties that Hart and Bruck obtained utilizing ATSM 8 [5] and ASTM E466 [6], as well as the layout of their center crack panel specimens. The Modulus listed for the material is 70.9 MPa, the yield at 2% offset is 116 MPa, and the parameters α and n at 9.9 and 0.22 respectively.

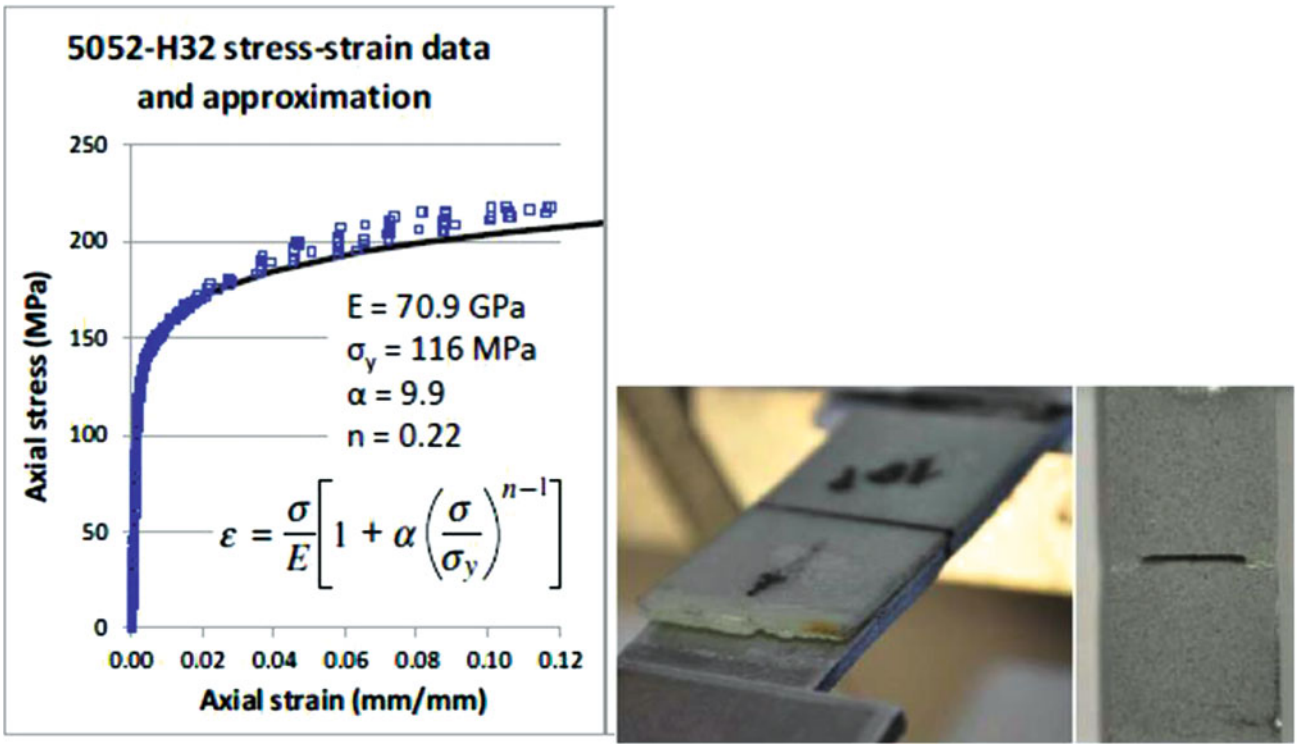

Fig. 2 5052-H32 Material properties and Specimen Failure [5]

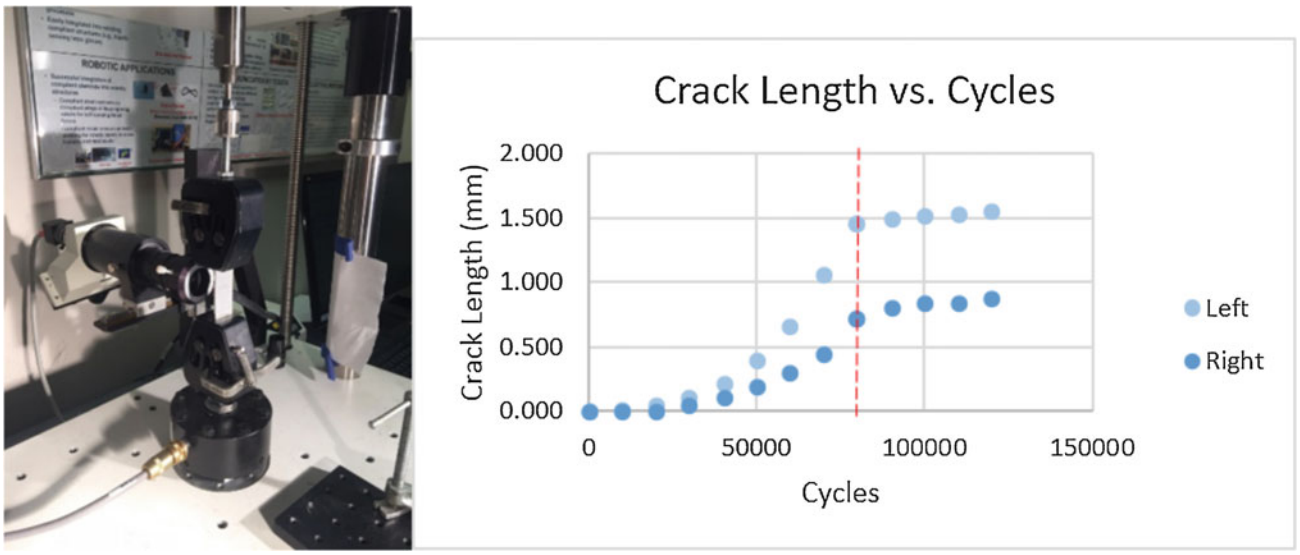

Fig. 3 Initial Specimen Setup

Initial experiments were carried out on this setup for this work, but the results indicated that there was an imbalance of crack growth between the left and right cracks growing from the notch during fatigue loading. Figure 3 above displays the friction wedge grip setup, as well as the crack length visually captured via microscope measurements, the left and right cracks shows differences over 0.5 mm at 80 k cycles. However, one of the promising results from these experiments was that the setup captured effects of crack growth when a high frequency pulse was applied at 80 K cycles, the crack growth shows a variation of the crack growth rate (Da/DN) before and after the pulse is applied.

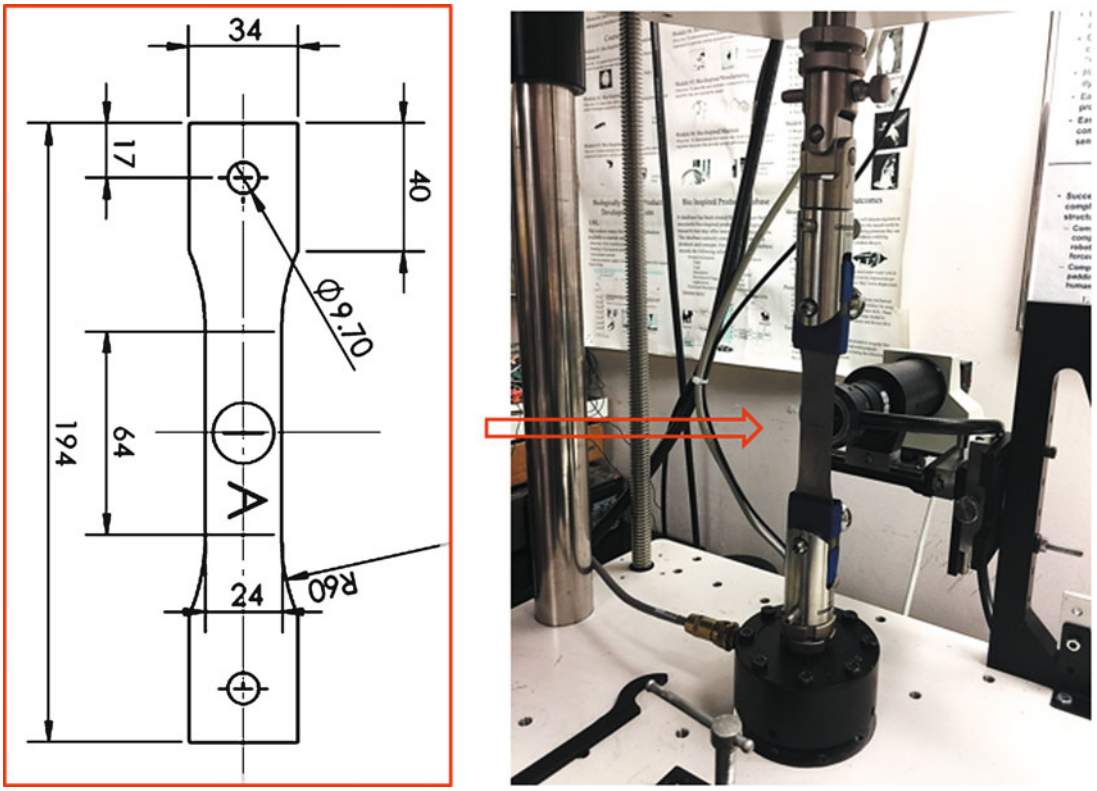

Fig. 4 Clevis Pin Specimen and Setup

It is important to mention that whereas the experiments by Hart and Bruck utilized a four post MTS servo hydraulic setup since they were interested in the ultimate loading capacity, this work work required flexibility to apply smaller loads with different characteristics, hence a two post Bose ElectroForce frame was used, which has the capacity of applying loadings up to 100 Hz and 3000 N. This device has a built in displacement meter with errors of less than 5 μm, and it has a block waveform generation software that allows for the implementation of unique load signals. Fast Fourier Transforms methods were utilized to ensure that the programmed signal and the applied signals displayed the required frequencies.

The specimen configuration shown in Fig. 4 was developed and it is an amalgamation of several ASTM methods, this was conducted to address the significant asymmetry observed with crack growth as previously described. ASTM E8 [5] guidance was utilized to develop the specimen tapers towards test region, while ASTM E647 [7] middle tension specimen configuration was utilized to size the center notch and test region, maintaining the configuration carried out by Hart and Bruck. Since a clevis pin was utilized, ASTM E338 [8] was utilized to develop end reinforcements and alignment tabs for the end pin connections to ensure the failure would not occur in or adjacent to the clevis pin area. Electrical Discharge Machining (EDM) techniques were utilized to manufacture the specimens, providing a stable level of accuracy for the component geometry, it was also critical to ensure alignment of end pins and size and location of center notch. Several test were carried out in this setup, along with finite element analysis, and microscope evaluations of the clevis pin areas and tapers to ensure no failure was visible and that crack growth would be focused towards the test region and adjacent to the notch. The material for the specimen in marine grade aluminum 5052-H32, with a nominal thickness of 2.29 mm (0.09in) Fig 4. Also shows how the clevis pins were utilized in the loading train, and end adaptors that were used to interface with the Bose frame and to help with specimen load alignment, Universal Grip LLC. components were utilized for this setup: Adapter—Male Bolt 5/8″-18 w/1″ length, Universal Joint Adapter; in addition, Mark-10 G1090 high capacity clevis grip (pair) were utilized. The load capacity of the members was at a minimal load of 9KN, hence far exceeding the capacity of the Bose equipment of 3KN, and ensuring no failure could be accidentally induced to the Bose fixture from a failure of the adapters under load.

The experimental setup consisted of several components setup to achieve two goals: observe/capture the crack growth on the back of the specimens using a microscope, and to capture the surface strains on the front face of the specimen utilizing digital image correlation techniques. Figure 5 below details the setup utilized for these experiments.

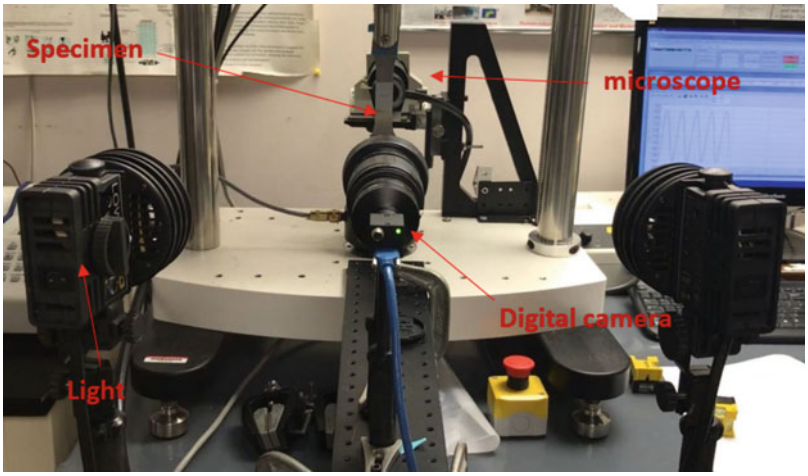

Fig. 5 Experiment Setup

In the back face of the specimens, an optics zoom inspection microscope head by Edmunds Optics was used, along with a Dolan-Jenner MI-150 fiber optic illuminator with a fiber optic ring light accessory, was utilized to capture the crack growth on the back side of the specimen. The setup was connected with a rack and pinion positioning system that allowed movement of the microscope along three axis via a hand knob, hence allowing the positioning of the microscope in different locations to capture crack growth. The microscope was able to visualize square areas of 0.5 mm on each side. Several digital pictures were taken on each crack emanating from each notch, which overlapped, and then were stitched together to form an overall view of the crack of the specimen.

In the front face of the specimen, a Point Gray Flea FL3-U3-88S2C-C digital camera attached to a Tamron 28–80 mm f/3.5–22 lens and adapter was used to capture static pictures of the surface of the specimen. In addition, two 250 W halogen Lowel Pro Lights were utilized to provide lighting to the specimen. The lights were not directly aimed at the specimens, but instead aimed at locations adjacent to the mid-point of the specimen, and focused as to provide evenly dispersed light flooding on the specimen. Digital Image Correlation (DIC) was utilized on the front face of the specimens to capture field surface strains [9], in order to capture these images, the area had to be prepped to generate distinct patterns that can be captured with PointGrey FlyCap 2 V2.11.3 and processed utilizing VIC-2D Ver6.0.6 by Correlated Solutions (Lexington, SC).

The figure below shows the typical DIC pattern applied, the generation of this pattern is achieved by first applying a coat of flat white paint as the background, and the black speckle patterns was developed by not directly applying paint, but instead relying on lightweight particles that slowly settle over the specimen. This procedure requires practice as the specimens needs to be rotated over multiple passes, ending with a specimen that has an adequate gray scaling and consistent patterns that would allow for acceptable DIC measurements. Several references were utilized to obtain best practices and recommendations on acceptable DIC techniques to obtain feasible results, one such body of work in conducted by the internationals digital image correlation society [10] (Fig. 6).

Experiment Protocol and Matrix

In order to explore the variability of the high frequency pulses, a couple of items das to be developed, first was a consistent process/protocol that was repeatable across experiments, and second was an experimental matrix that varied certain parameters to determine their influence on the response. Figure 7 below outlines the experimental process utilized. It is worth noting that each step below is a top level overview, as there are substantial details on each step that are needed for consistency, i.e. the number of photographs taken during measurements, camera settings, etc.

The specimen preparation was the initial step in the configuration, the back side of the specimens that faced the microscope was polished to a mirror type finish, this aided in the identification of the crack tip. The front of the specimens received a DIC spackle pattern that had a sigma level equal or below 0.001 [9]. The sigma level was tested during the baseline measurements stages until the desired value was achieved. Prepping the specimens several times was required in some cases to achieve

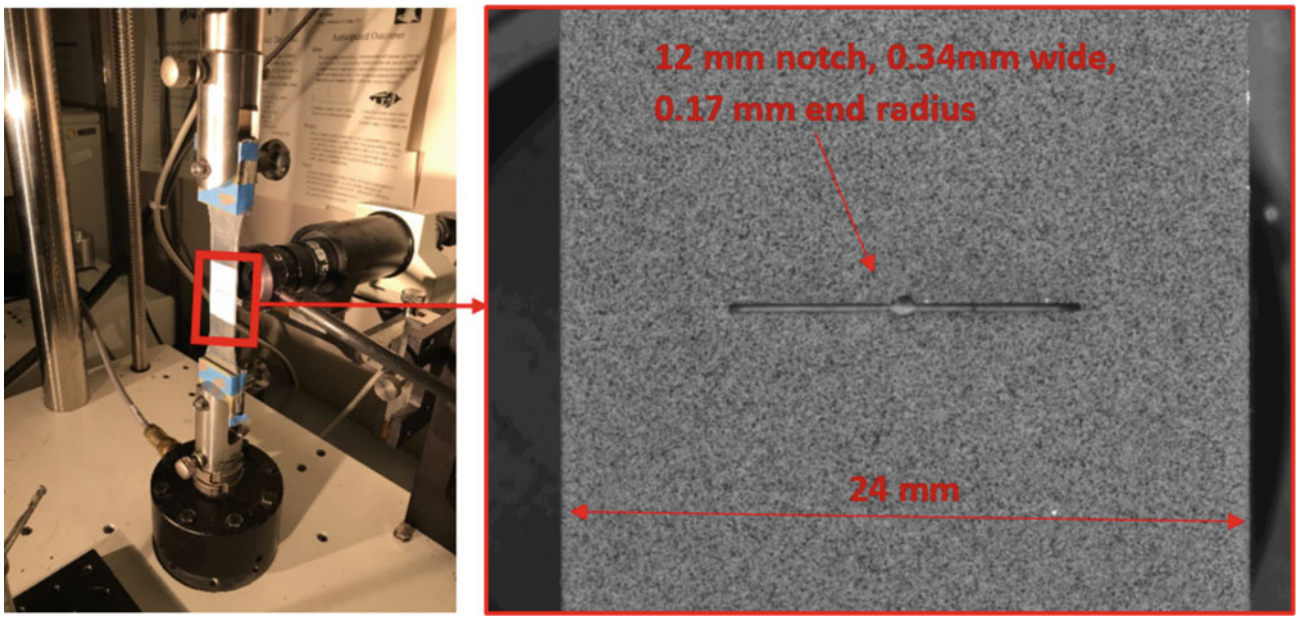

Fig. 6 Specimen and Speckle Pattern

Fig. 7 Experimental Process

the desired values, as inconsistent baseline measurements would result in unpredictable data during the later stages of the experiments. The baseline measurements also consisted on utilizing DIC to evaluate the displacement of the fixture. i.e. if the load frame indicated a 0.2 mm displacement, do the DIC measurements also show a similar value? This was done by only pining the stationary end of the specimen and comparing the displacement between the load frame and DIC calculations. Additional baseline measurements included static DIC measurements at 200, 1100, and 2000 N, as well as microscope crack measurements at no load and 2000 N. The initial crack growth was a step used to develop a crack and go outside the envelope of the stress-strain effects of the notch radius [11]. The notch radius was 0.17 mm, and an initial starter crack was developed to be around 0.5 mm in length. The HF pulse was applied at 40 K cycles, subsequent measurements monitored the crack growth rates after the HF pulse was applied to evaluate the recovery. It is important to note that the load ranged from 200 N to 2000 N, where the stress ratio $R = 0.1$, the frequency used for fatigue was 5 Hz, and the nominal Stress intensity $\Delta K = 6.07$ MPa-m$^{0.5}$.

The experimental matrix utilized is shown in the table below, it consists of a baseline test where no HF pulse is applied, and a 3×3 matrix with three level and two factors (amplitude, frequency), resulting in nine treatments, where the amplitude of the pulse is increased in 1/3 amplitude increments, and frequencies that range between 4 and 10 times the baseline frequency i.e. specimen 3C had a peak amplitude of 2900 N, and an HF pulse with a frequency of 50 Hz.

For this matrix, the HF pulse was only applied at the peak of the ordinary wave of 5 Hz, hence the phase shift was held constant, as well as the log decrement of the function as maintained at 0.21. Introduction of other factors would increase the matrix size to a 3^3 design resulting in 27 treatments.

Initial Results

The initial results provided adequate results, but also highlighted areas of the experiments that required tuning to capture the desired data. Figure 8 below outlines the crack length results of three experiments and the baseline. The frequency is contact at 20 Hz, but the amplitude is varied for each experiment. It can be seen that after the HF pulse is applied at 40 K cycles, the

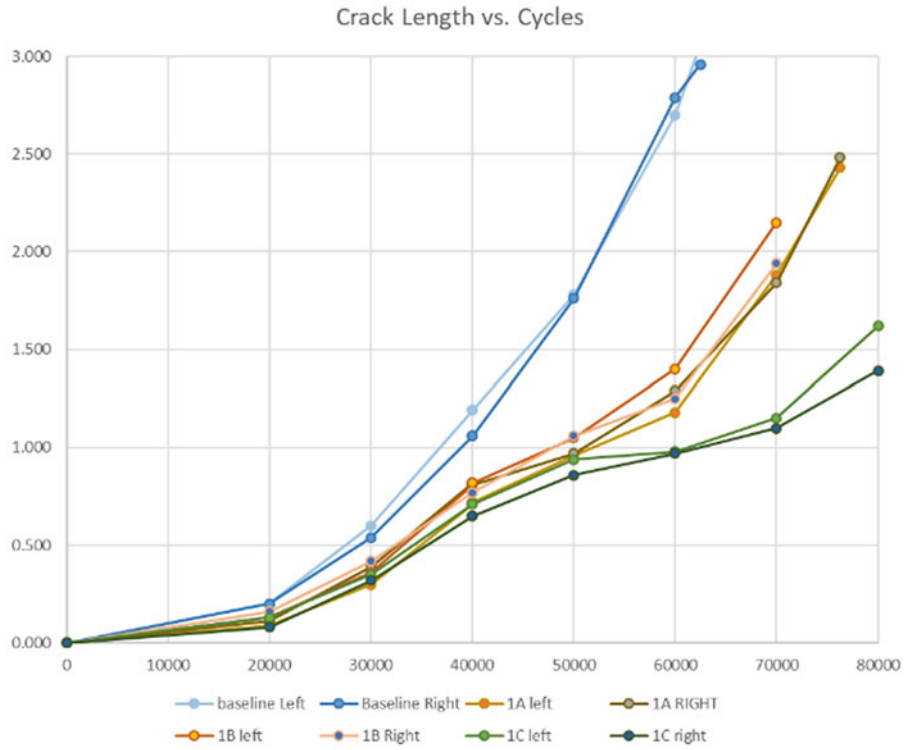

Fig. 8 Initial Results, Amplitude Variability, 20 Hz

crack growth rate is different over time as compared to the baseline, with block 1C (20 Hz, 2900 N) displaying the longest recovery. These measurements are based on microscope measurements of the crack length on the left and right side of the crack.

Reviewing the DIC measurements with Vic2D on the front side of the specimens, one can see variation on the strain fields and crack length and dA/dn as shown in Fig. 9 below.

The data results indicate that a higher fidelity was needed in order to capture the behavior, the data acquisition of every 10 K cycles does not provide sufficient fidelity to address the underlying behavior observed. At the core of this work, models by Wheeler [12] and Willemborg [13]. These models look at the plastic zone behavior, Wheeler relying on crack growth rates, and Willemborg utilizing stress intensity for the calculation, as follows (Fig. 10).

More recent research work by Mehrzadi & Taheri [14], and Chen [15] outline the behavior of the plastic zone ahead of the crack tip.

The common thread of all these models is that an overload plastic zone is created once an overload/underload occurs, and the magnitude of this region has an effect on the crack growth rate as long as the cyclic plastic zone stays within its boundaries. In our case, the data obtained indicated that an overload zone is created, but the fidelity of the data does not support the identification of its progression over time. In addition, it is critical to identify the location of the crack tip with respect to the plastic zones around it.

Data Processing

Of the two limitations outlined above, data fidelity improvements can be addressed by capturing a higher number of data points, instead of capturing data every 10 K cycles, capturing data ever 2 K cycles. The drawback of this approach is that the data required for processing increases in magnitude for each test, hence a more robust/automated method of identifying the crack tip location and plastic zone behavior is needed. A unique method for using DIC for crack detection was developed by Bruck [16] while utilizing curve fitting to locate the crack tip location based on the vertical displacement field. Other researchers have tackled this problem, such as Yates who evaluated the vertical displacement field ahead of the crack tip

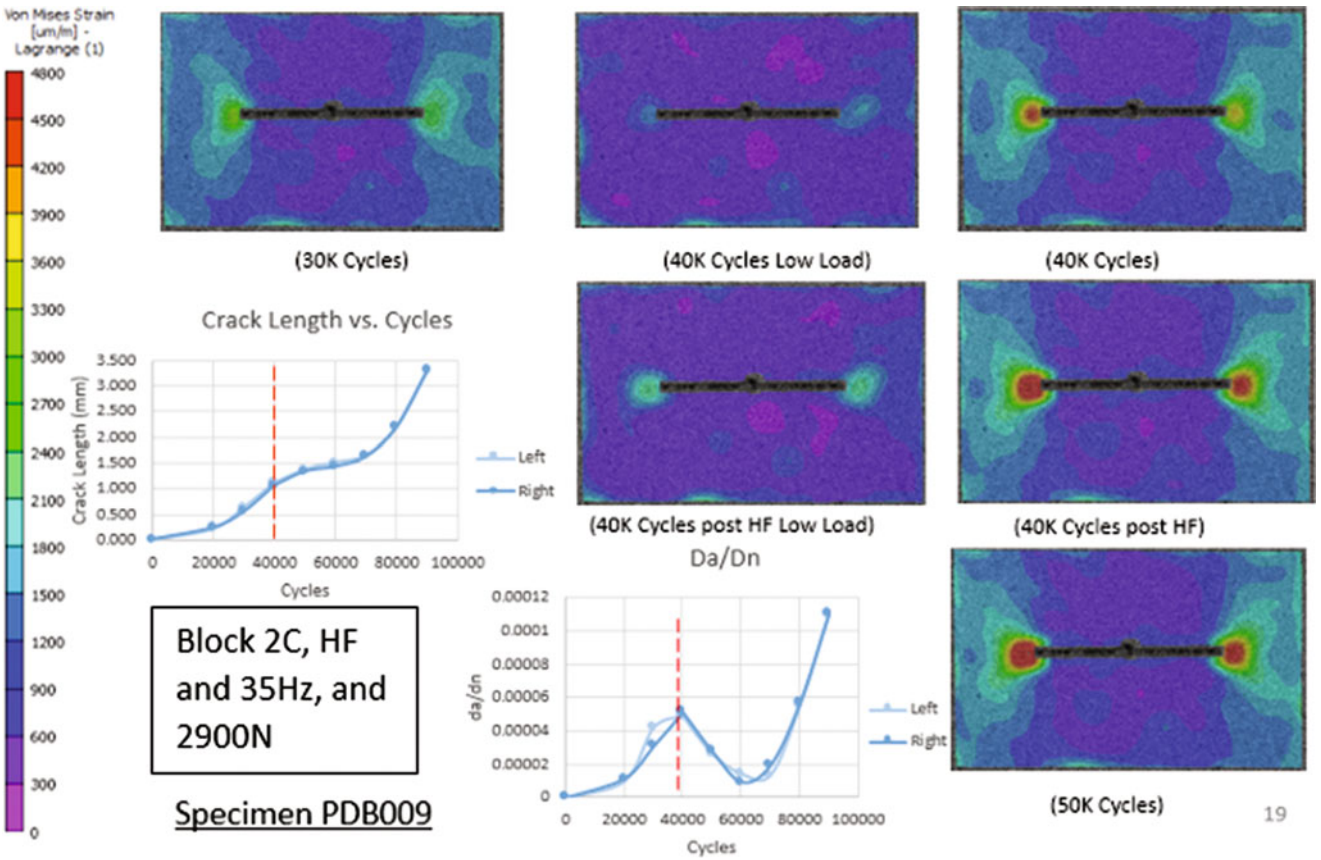

Fig. 9 Block 2C at HF of 35 Hz and Peak Amplitude of 2900 N

Wheeler:

$$\frac{da}{dN} = \Phi_R \left(\frac{da}{dN}\right)_{CAL}$$

$$\text{where}: \Phi_R = \begin{cases} \left[\frac{r_{p,i}}{a_{OL}+r_{p,OL}-a_i}\right]^m & \text{when} \quad a_i + r_{p,i} < a_{OL} + r_{p,OL} \\ 1 & \text{when} \quad a_i + r_{p,i} > a_{OL} + r_{p,OL} \end{cases}$$

Willemborg:

$$\frac{da}{dN_i} = \frac{C(\Delta K_{eff})_i^m}{[(1-R_{eff})_i]K_c - (\Delta K_{eff})_i}$$

Fig. 10 Wheeler and Willemborg Models

[17]. Since the vertical displacement gradient ahead of the crack tip is much higher than other zones, a threshold can be set based on the gradient, and hence, a crack tip location can be obtained.

This work included extracting DIC output data to MATLAB in order to program algorithms to find the crack tip location. The process for this extraction included exporting output vectors (x, y, V, U, Von Mises strain) from DIC at various pixel locations, for each load set (200, 1100, & 2000 N), and time step (30 K, 32 K cycles, etc.). This data was then brought into MATLAB, where it was arranged in matrix form, and the gradient of V along the vertical direction was calculated. Once this was completed, data could be processed for visualization, where the maximum gradient can be picked from each slide of the notch in the vertical direction. The figure below shows the gradient calculated plotted along the Z axis, hence providing a unique method to visualize the behavior around the crack tip by. Figure 11 below outlines how the data can be plotted in 3D, and then filtered to show a specific range.

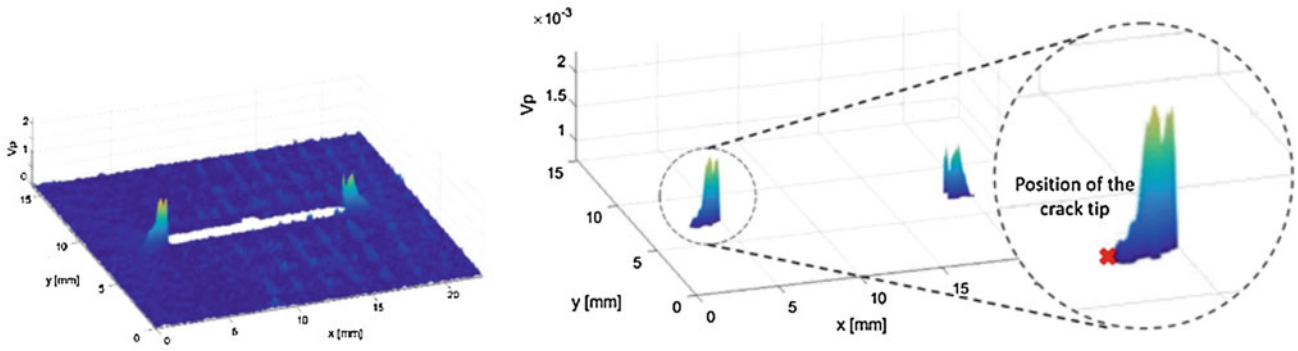

Fig. 11 Vertical Gradient Vp

This data can also be used to determine the crack path and other output vectors further analyzed to automatically show Von misses strains when compared with the crack tip location. This is a unique way to visualize the behavior shown by Yates et al., uniquely developed to process the output experimental data.

This methods also provides a unique process for the identification of the plastic zone areas and begin the comparison with theoretical models [18] where the approximate size of the plastic zone as a function of angular position, r(ϑ), can be estimated by formulations that are based on yield criterion, as follows:

$$r(\theta) = \frac{1}{4\pi}\left(\frac{K_I}{\sigma_y}\right)^2 \left(\frac{3}{2}\sin^2\theta + \cos\theta + 1\right)$$

$$r(\theta) = \frac{1}{4\pi}\left(\frac{K_I}{\sigma_y}\right)^2 \left(\frac{3}{2}\sin^2\theta + \left(1-\nu^2\right)^2 (1+\cos\theta)\right)$$

While the work on outlined above displays the complex shapes of the plastic zones under plane stress and plan strain conditions, these items can be simplified to a circular zone ahead of the crack, as shown by Chen [15].

Experimental Results & Follow on Work

The data captured now allows a visualization of the evolution of plastic zones with respect to the crack tip location, Fig. 12 below shows the effects of block 2C which had a HF pulse of 35 Hz and 2900 N in magnitude. The application of this small pulse showed a change is the residual strain ahead of the crack tip and the loaded strain paths. It also allows the inclusion of the calculated crack path using the strain gradient value in the system.

Work was carried out to compare the error values obtained between microscope measurement and DIC calculated values. Figure 13 below displays the horizontal crack length measurements for the crack propagating form each notch (left and right). The timeline of interest ranges from 36 K cycles to 62 K cycles.

Another aspect of the work is evaluating the failure mechanism observed, while the microscope measurements provide a view of the crack propagation, a Barker's etch method [19] was used for anodizing the aluminum alloy, and then utilizing optical microscopy with polarized lights to observe the grain boundary and the propagated crack. Figure 14 below displays results at 500 μm, 100 μm, and 20 μm magnification levels, allowing the evaluation of the crack propagation through the grain, and the investigation of shielding effects such as contact and deflection on crack growth [20].

The work presented has resulted in procedures utilizing DIC for capturing and quantifying details of the fatigue crack growth associated with HF pulse loading. In future work, the dimensions of the HF pulse plastic zone can be captured, and then further utilizing the DIC data, it will be possible to show the plastic zone progression and change over time to evaluate the applicability of failure models such as Willemborg. Another important aspect will be how the added definition of the plastic zone observed affects the crack path. There are several instances, such as the data in Fig. 13, where there is a

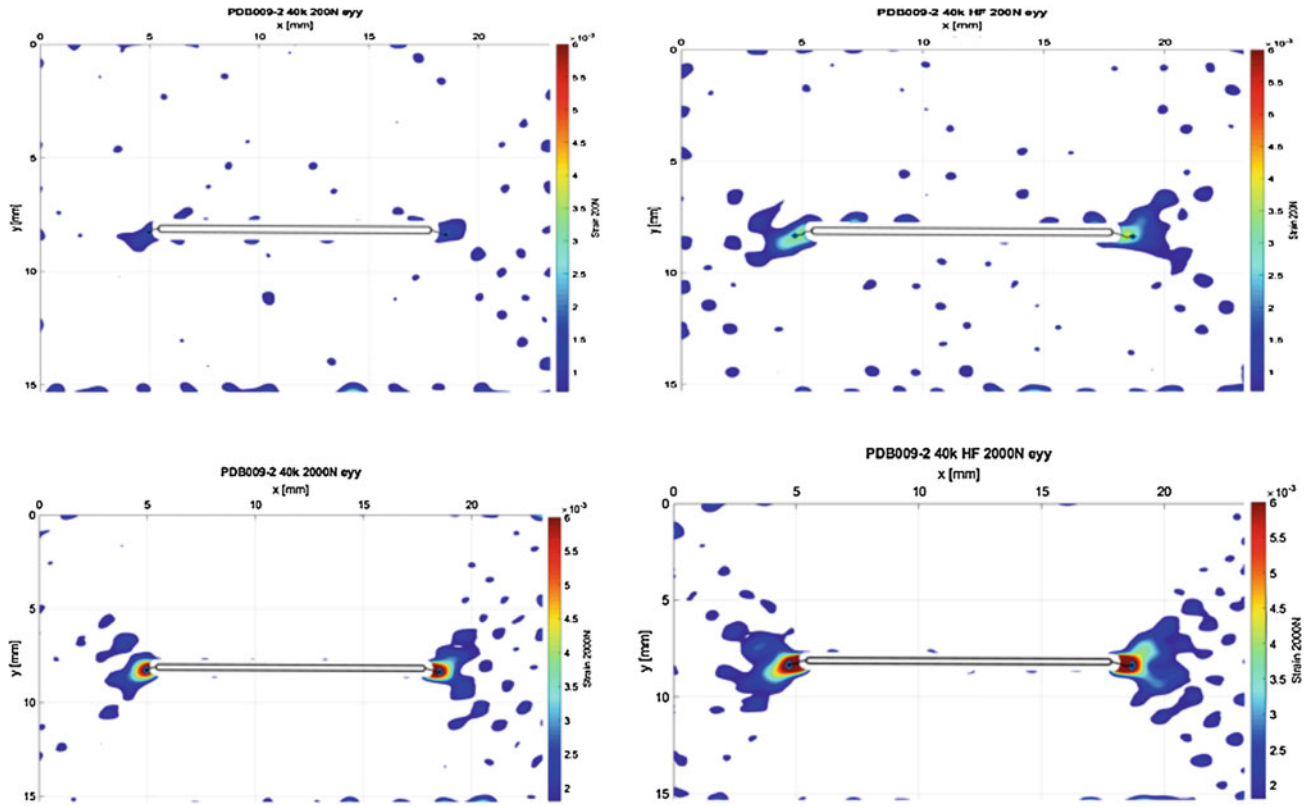

Fig. 12 *eyy* strain pre and post Block 2C at HF of 35 Hz and Peak Amplitude of 2900 N

Table 1 Experimental matrix

		High Frequency Pulse Amplitude (N)		
	Baseline, No Effects	1/3 Peak Amplitude 2300	2/3 Peak Amplitude 2600	Peak Amplitude 2900
High Frequency Pulse Frequency (Hz)	4× Main Wave 20	1A	1B	1C
	7× Main Wave 35	2A	2B	2C
	10× Main Wave 50	3A	3B	3C

deviation of the crack path direction following the occurrence of the HF pulse, where strain fields surrounding the crack tip can be taken into consideration to understand the origin of the deviation. Finally, the experiments in Table 1 can be expanded to obtain higher fidelity of data post the application of the high frequency pulse.

Conclusions

Existing models, like the Wheeler, Willemborg, and variations of these, have been utilized to predict the crack growth behavior with varying degrees of success. In this study, we created experimental matrices to explore the effects of overload/underload combinations on fatigue crack growth in 5xxx aluminum, typically used in marine applications. Both visual inspection of crack tip location, and using Digital Image Correlation (DIC) techniques for characterization of the crack tip deformation fields. These techniques were used on a designed center crack tension (CCT) panel specimens to measure

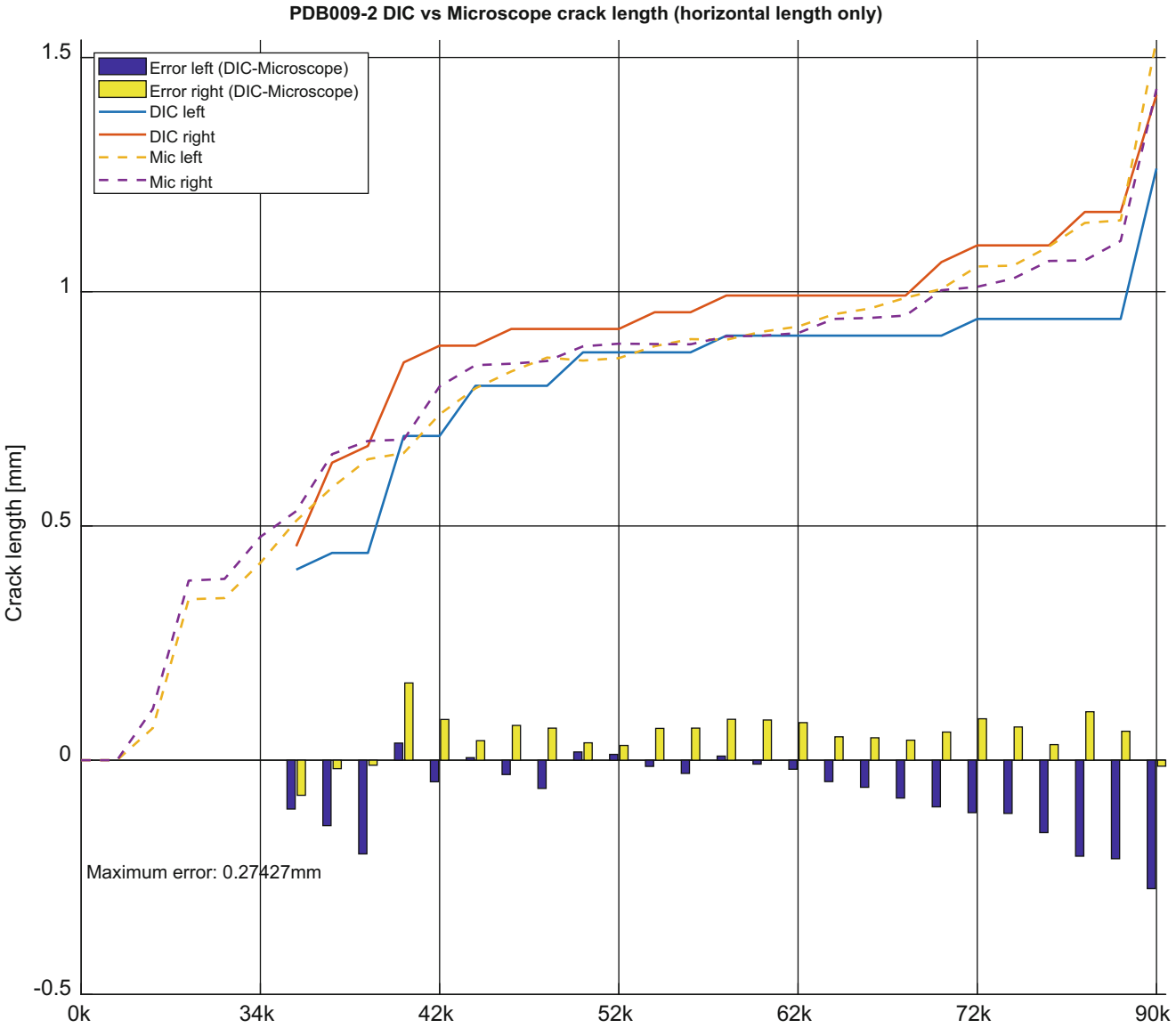

Fig. 13 comparison of DIC and microscope crack length, Block 2C at HF of 35 Hz and Peak Amplitude of 2900 N

crack growth. DIC techniques also enabled additional analysis of strain fields to elucidate on the conditions responsible for the change in the crack growth behavior. The development of the experimental protocol was critical for capturing the desired output data for DIC and microscope measurements, and observe the behavior of the plastic zones surrounding the crack tip. Several experiments were conducted until a finalized methods that captured the required data was developed. Unique MATLAB algorithms provided a means to develop innovative approaches to automatically capture the crack tip location and display it along with observed behavior around the crack tip. The next phase of this work includes utilizing this observed data to elucidate the mechanics of crack growth behavior when affected by an embedded high frequency load models for fatigue crack growth.

Acknowledgements Work described was performed by the Naval Surface Warfare Center Carderock Division's Survivability, Structures, Materials Department, and University of Maryland College Park's Department of Mechanical Engineering. Financial and technical support was provided by an NSWCCD In-house Laboratory Independent Research (ILIR) program under Dr. Jack Price, and a grant provided to UMD by program officer Dr. Paul Hess of the Office of Naval Research Code 331 under grant number N000141812016.

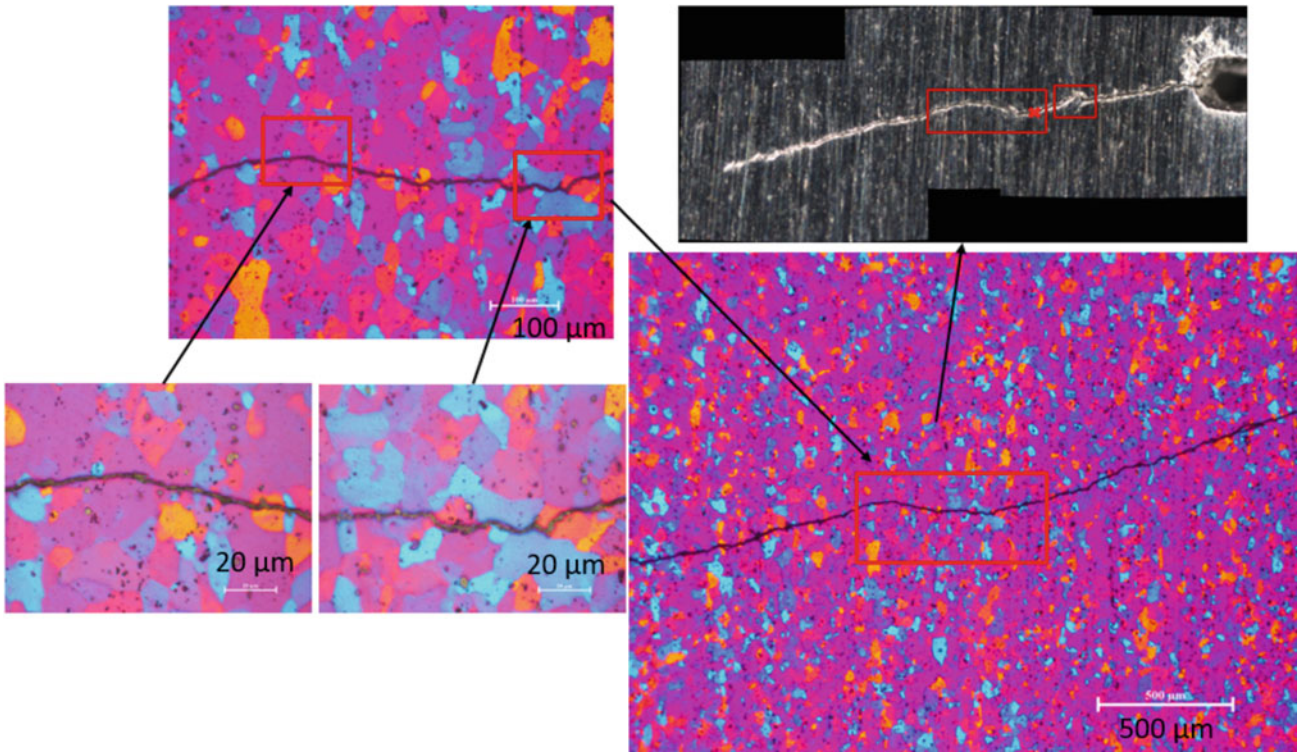

Fig. 14 Barkers Etch of Specimen, Block 2C, HF at 35 Hz and 2900 N

References

1. R. Murthy, G. Palani, N. Iyer, State-of-the-art review on fatigue crack growth analysis under variable amplitude loading. J Inst Eng (India) **85**, 118–129 (2004)
2. Y. Sumi, Fatigue crack propagation in marine structures under seaway loading. Int. J. Fatigue **58**, 218–224 (2014)
3. W. Fricke, H. Paetzold, Experimental Investigations on Fatigue Damage of Ship Structures Caused by Whipping Stresses, in *PRADS*, (Korean Society of Naval Architects, Changwon City, 2013)
4. D. Hart, H. Bruck, Characterization and modeling of low modulus composite patched center crack tension specimen using DIC surface. Fracture Fatigue Failure Damage Evolution **6**, 31–43 (2018). in Society of Expermiental Mechanics
5. ASTM-E8, *ASTM E8M-08: Standard Test Methods for Tension Testing of Metallic Materials* (ASTM International, Conshohocken, 2008)
6. ASTM-E466, *ASTM E466–07: Standard Practice for Conducting Force Controlled Constant Amplitude Axial Fatigue Tests of Metallic Materials* (ASTM International, Conshohocken, 2007)
7. ASTM-E647, *Standard test method for measuring fatigue crack growth rates* (ASTM International, Conshohocken, 2015)
8. ASTM-E338, *Standard Test Method of Sharp-Notch Tension Testing of High-Strength Sheet Materials* (ASTM International, Conshohocken, 2003)
9. M. Sutton, J.-J. Orteu, H. Schreier, *Image Correlation for Shape, Motion, and Deformation Measurements* (Springer LLC, New York, NY, 2009)
10. E. Jones, *Good Practices Guide for Digital Image Correllation* (International Digital Image Correllation Society, Portland, OR, 2018)
11. J. Bannantine, J. Comer, J. Handrock, *Fundamentals of Metal Fatigue Analysis* (Prentice Hall Inc, Upper Saddle River, NJ, 1990)
12. O. Wheeler, Spectrum loading and crack growth. J. Basic Eng. **94**, 181–186 (1972)
13. J. Willenborg, R. Engle, H. Wood, *A crack growth retardation model using an effective stress concept, AFFDL TM-71-1-FBR, Jan 1971*, (1971)
14. M. Mehrzadi, F. Taheri, A material sensitive modified wheeler model for predicting the retardation in fatigue response of AM60B due to an overload. Int. J. Fatigue **5**, 220–229 (2013)
15. F. Chen, F. Wang, W. Cui, Fatigue life prediction of engineering structures subjected to variable amplitude loading using the improved crack growth rate model. Fatigue Fract Eng Mater Structures **35**, 278–290 (2012)
16. H. Bruck, *Analysis of 3-D Effects near the Crack Tip on Rice's 2-D J-Integral Using Digital Image Correllation and Smoothing Techniques*, M.S. Thesis, Univeristy of South Carolina, (1989)
17. J. Yates, Y. Zanganeh, Quantifying crack tip displacement fields with DIC. Eng. Fract. Mech. **77**, 2063–2076 (2010)
18. E. Gdoutos, *Fracture Mechanics, An Introduction, Second Edition* (Springer, Minneapolis, 2005)
19. E. Cerri, E. Evangelista, *Metallography of Aluminum Alloys* (Mechanical Engineering Department, European Aluminum Association, Ancona-Italy, 1999)
20. R. Ritchie, Mechanisms of fatigue crack propagation in metals, ceramics and composites: role of crack tip shielding. Mater. Sci. Eng. **A103**, 14 (1988)